Check for updates

ADVANCED MATERIALS TECHNOLOGIES
www.advmattechnol.de

3D Printing of Implants Composed of Nanjing Tamasudare-Inspired Flexible Shape Transformers

*Tetsuhiko F. Teshima, Lukas Hiendlmeier, Korkut Terkan, Sabine Zips, Leroy Grob, Francisco Zurita, Philipp Rinklin, and Bernhard Wolfrum**

Minimizing damage during the insertion of stents or other medical devices is critical for rapid and successful recovery. Since the delivery passages are often narrower than the size of the delivered object, a high deformability of the implanted devices is paramount to achieve a smooth insertion into the target tissue. In this study, a novel design of 3D-printable and highly deformable structures inspired by Nanjing Tamasudare is proposed. These structures rapidly change dimensionality from flat to linear, elongated shapes. A series of single units that each comprises two interconnected rods and attaching loops are directly 3D-printed without classical assembly or fabrication. Multiple units are connected together but remain individually movable and deformable. The smooth changes of the unit assembly, including shifting, bending, and inclination, allow to transform the structure from an initially condensed state to various types of target shapes. To verify the transformation capabilities, smooth insertion of the 3D-printed structure in a mock-up vessel through a small opening in an elongated state is demonstrated. After insertion, the units are reassembled to a stent-like structure within the vessel. The authors believe that this 3D-printable and highly transformable design is widely applicable for insertion operations of implantable devices or electronics.

1. Introduction

Implantable medical devices such as stents and bioelectronic implants find numerous applications for health monitoring[1] as well as in vivo therapy,[2] surgery,[3] and rehabilitation.[4] Since the application of these devices requires them to be inserted into the body, minimal invasiveness and seamless interpenetration are key features for reducing the clinical burden and allowing a rapid recovery of patients.[5] To address these challenges, it is important to miniaturize the implants in order to make them catheter- or syringe-inducible.[6] To insert objects which ultimately need to be larger than the delivery passage, they should be transformed to a smaller and thinner state during the delivery.[7] The narrower the delivery passage becomes relative to the size of the delivered object, the more compromises must be taken for selecting materials and design.

Integrating soft and functional materials with miniaturization technology has taken significant strides in confronting this challenge.[8] In particular, shape-memory materials with a characteristic time-transient change in morphology in response to external stimuli achieve high deformability and shape recovery function throughout the delivery process.[9] 2D, shape-memory, and microporous mesh electrodes were photo-lithographically fabricated, loaded into a syringe, and injected into the brain.[10] While being compressed to a quasi- 1D shape during the delivery phase via syringe injection, the meshes subsequently relaxed and expanded to regain their original 2D shape. To further increase the dimensionality of the implants, origami-[6,11] or kirigami-inspired[12] folding elements have been incorporated with additive manufacturing techniques to allow for shape-changes from 2D planes to 3D final structures. In particular, 3D-printing of shape memory polymers facilitated a direct fabrication of patient-customized stents.[13] For instance, bifurcated stents with a kirigami structure smoothly travel inside the vessels in a folded state and be unfolded successfully in their ultimate position through external stimulation.[12] However, conventional origami- or kirigami-inspired devices only reach simple final 3D geometries, which are limited by the intrinsic substrate structure. Therefore, it is required to improve the shape transformability and reach higher aspect ratios between the pristine and deformed state. This technological improvement will lead to a wide variety of applications including biomedical devices such as transformable electronics and stent devices.

In this study, we propose a 3D-printable design of individual elements inspired from highly deformable Japanese performance tools, termed Nanjing Tamasudare (alternatively called Nankin Tamasudare; "Nanjing," the name of

Dr. T. F. Teshima, L. Hiendlmeier, K. Terkan, S. Zips, Dr. L. Grob, F. Zurita, Dr. P. Rinklin, Prof. B. Wolfrum
Munich School of Bioengineering
Department of Electrical and Computer Engineering
Technische Universität München
Boltzmannstraße 11, 85748 Garching, Germany
E-mail: bernhard.wolfrum@tum.de

Dr. T. F. Teshima, L. Hiendlmeier, F. Zurita, Prof. B. Wolfrum
Medical & Health Informatics Laboratories
NTT Research Incorporated
940 Stewart Dr, Sunnyvale, CA 94085, USA

The ORCID identification number(s) for the author(s) of this article can be found under https://doi.org/10.1002/admt.202100240.

© 2021 The Authors. Advanced Materials Technologies published by Wiley-VCH GmbH. This is an open access article under the terms of the Creative Commons Attribution License, which permits use, distribution and reproduction in any medium, provided the original work is properly cited.

DOI: 10.1002/admt.202100240

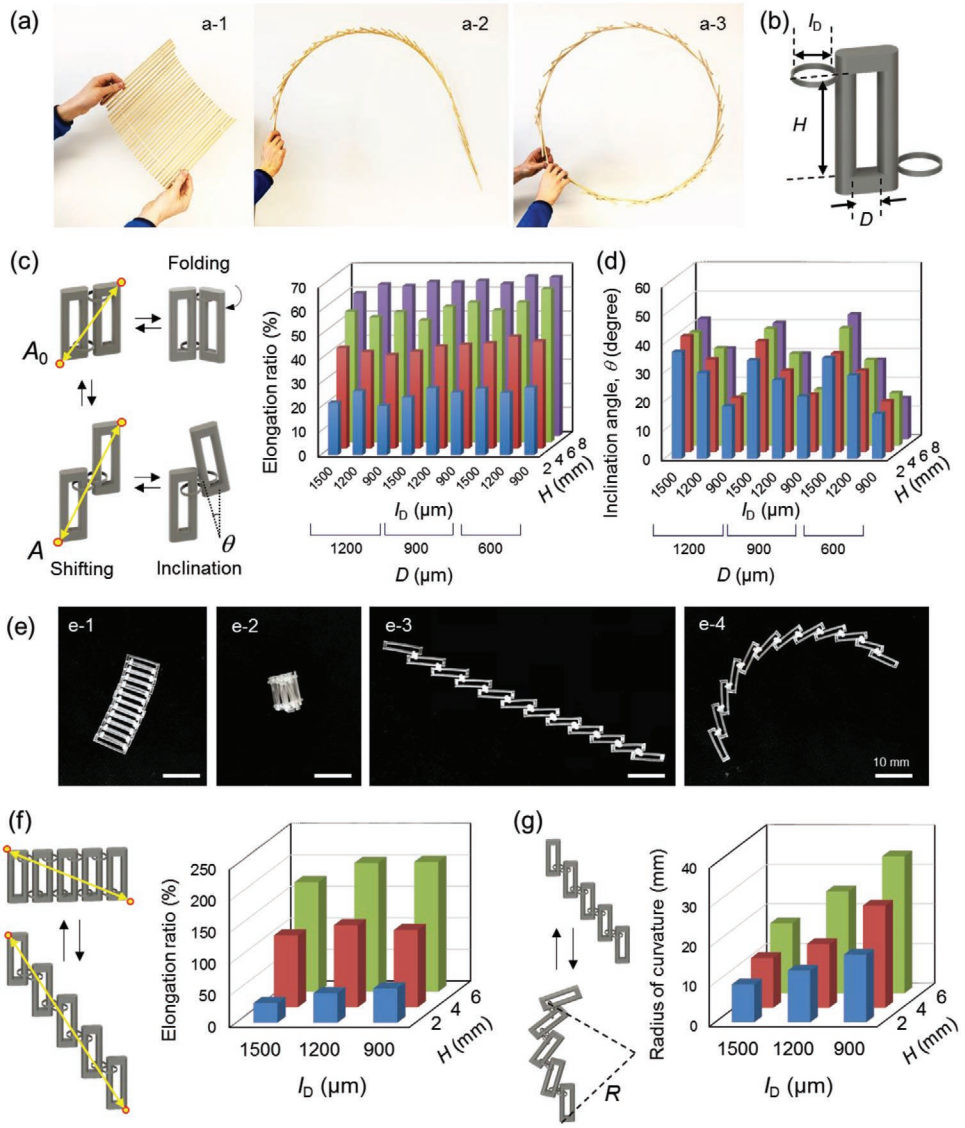

Figure 1. Nanjing Tamasudare-inspired transformation (NTTr). a) Sequential images of deformed Nanjing Tamasudare tools. The tools can be shifted for elongation and inclined to form tubular shape. b) Schematic illustration of individual NTTr units. Schematics illustrating the three types of movements. c) Experimentally measured elongation ratios and d) inclination angles of NTTr units that were assembled in a pair. e) A series of images of 3D-printed samples. e-1) The units in the original state e-2) were folded, e-3) shifted, and e-4) then inclined. Schematic images illustrating NTTr units that were assembled to be aligned in a serial configuration, and f) corresponding elongation ratios and g) radii of curvature.

the capital of Jiangsu province, China; "Tamasudare," woven screen blinds). In principle, the tools are composed of loosely woven bamboo sticks. They can be twisted, folded, or extended to portray objects and quickly brought back to their original shape for the purpose of traditional performing art (**Figure 1**a). Here, the individual elements of Nanjing Tamasudare-inspired Transformers (NTTr) comprise single cylindrical rods with two loops attached (Figure 1b). When these elements are assembled in series, the combination of rods and loops permits their deformation into several distinct shapes: shifting in length between two ends to form a 1D fiber structure, bending of the fiber structure, and back-transformation to the initial structure. Multiple connected NTTr units form complex 3D structures like stents and expandable mesh designs. These devices are transformed to a linear shape for the delivery through a narrow channel and then reconstructed to the final 3D structure at the desired position. The combination of these movements enables an expandable design while remaining minimally disruptive to the native body material during insertion. Although the traditional assembly technique is impractical for fabricating and connecting small devices, 3D-printing techniques are able to produce microscale, interconnected, and loop-shaped structures in a batch process using a wide range of photocurable materials. This design of NTTr structures is universal and might be applicable to other types of 3D printing technologies,[14] including high-resolution two-photon polymerization.[15] Due to the flexible changes in dimensionality, we envision that NTTr will emerge with complex geometries and

© 2021 The Authors. Advanced Materials Technologies published by Wiley-VCH GmbH

functional materials improving the success rate of minimally invasive insertion.

2. Results and Discussion

In the individual element of NTTr, a rectangular ring is made of a pair of two rods 600 μm in diameter with two loops attached. One loop is attached to one end of one side of the rod unit, and the other loop is attached at the other end on the opposite side of the rod. Each loop attachment has a ring shape. Although a single unit of an original Nanjing Tamasudare consists of one central rod and two strings, it is technically difficult to print the loop structure on a rod without overlapping it with loops on the next rod using conventional 3D-printing techniques (Figure S1, Supporting Information). As a readily printable alternative, we designed a rectangular-shaped base unit with attached loops for this study (the details of the design parameters are provided in Figure S2a and Table S1, Supporting Information). We fabricated the structures using digital light processing (DLP) 3D-printing with a constrained-surface configuration and customized blend resin of polyethylene glycol diacrylate and 2-isopropylthioxanthone[16] (PEGDA-ITX, details provided in Experimental Section).

The loop attachments on each rod allow multiple NTTr units to be connected. Sliding of the loops connecting two units facilitates the desirable change in dimensionality. Two rods within individual units are spaced apart, so that the loops on either side slide independently without any interference in the center region. A pair of two adjacent NTTr units arranged in parallel and connected by their loops can perform different kinds of motion, including shifting (displacement along the rod axis), folding (rotation around the rod axis), and inclination (rotation with respect to the rod axis) (Figure 1c). While the shifting distance is limited by the position of the loop attachments, which come into contact upon maximum displacement, the folding occurs until the rods are in direct contact. Last, inclination refers to a bending along the axes of the individual loops. While shifting and folding may occur independently, the inclination occurs only in the elongated state.

Shifting and inclination are regulated by the design parameters of single NTTr units. In particular, important independent design parameters are the distances between the first and second loop along the axis of the element (H), the distance between the adjacent rods (D), and the diameter of the attachment loop (I_D) as well as the rod diameter (Figure 1b and Table S1, Supporting Information). We minimized the difference between the design and the printed objects using a high-resolution PEGDA-ITX-resin. The distance from the lower-left corner of the first unit to the upper-right corner of the second unit increases from an initial value A_0 to a final value A upon shifting displacement (see Figure 1c). The elongation ratio $(A/A_0 - 1) \times 100$ ranges from 20% to 66% and depends on H. Furthermore, the inclination angle θ between two single units after elongation is controllable with the loop shape, I_D, wherein θ ranges from 14° to ≈42° (Figure 1d). Thus, the dimensional change and deformability are simply controlled by the loop shape and the position of their attachment, and ultimately these dimensions control how multiple units will be assembled into 3D structures.

Based on three basic motions in the paired units, a number of single units were connected in a straight line and shifted to transform from a flat 2D to an elongated 1D shape with high flexibility and reversible deformability (Figure 1e). After shifting, they formed a curved shape due to bending in one direction. While the deformability of elongation was only controlled by H (max. 205%), the minimum radius of curvature of the bent fibers was controlled by both H and I_D (min. 9.5 mm) (Figure 1f,g). The folding process enables the transformation from flat 2D shapes to closely packed and bent cylindrical shapes. The combination of these three deformations endows high transformability ranging from 1D fibers to complex 3D structures to the assembly of NTTr units.

To increase their volume, the assembled fibers were aligned in parallel and connected to each other. For simplicity, two units with equal lengths and structures were adjacently paired. The respective pairs of the two single fiber units were connected by a bridging board of length L (**Figure 2**a). The connected two fibers can be shifted, folded, and inclined simultaneously, which provides a particular final 3D structure. For instance, the bending motion allows for a curved formation of single fibers with a radius of curvature, R. The value of R is dependent on the diameter of the attachment loop, I_D, with larger attachment loops leading to smaller radii of curvature in the bent fibers (Figure 2b). In addition, the value of R can be regulated by the length of the bridging boards, L. Shorter boards increase the flexibility of the two fibers, leading to smaller radii of curvature (Figure 2c). A theoretical relation between R and the design parameters is given in the supporting information (structure deformation).

To generate a tubular stent-like structure, partially open loops were attached on the final units as reversible and detachable coupler hooks. These hooks connect both edges of the bent fibers to form stent-like shapes with lengths equal to those of the rods (Figure 2d and Figure S2, Supporting Information). After fixing with hooks, the connected fibers were transformed in a circular configuration and locked. The resulting radius R depends only on the inclination angle θ that is controllable with I_D. Similar to the bending motion, the combination of shifting and inclination also produced tubular structures with a length equal to L (Figure 2e). As observed in Figure 1c,g, R is regulated by I_D and the length of the rods. Shifting and inclination lead to an assembly of larger ring shapes compared with the bending motion. Since the inclined and bent states are reversibly switched, the shifted fibers can be endoscopically introduced, subsequently bent, and assembled into tubular stents inside the targeted tissue. Thanks to their high flexibility in scale, these transformable stents could potentially be used as the inner stent rings for bile ducts,[17] tracheae,[18] esophagi,[19] and gastrointestinal tracts,[20] and as outer rings to cover atrioventricular rings and prevent hypertrophy.[21]

A reduced density of connecting boards provides a higher flexibility in the final 3D structures. For example, more than two NTTr fibers were connected only at the edges and assembled in a joined-end configuration (Figure 2f). As a result, the paired units stretched in the lateral plane forming a caged structure with multiple dimensionalities. When four lines of

© 2021 The Authors. Advanced Materials Technologies published by Wiley-VCH GmbH

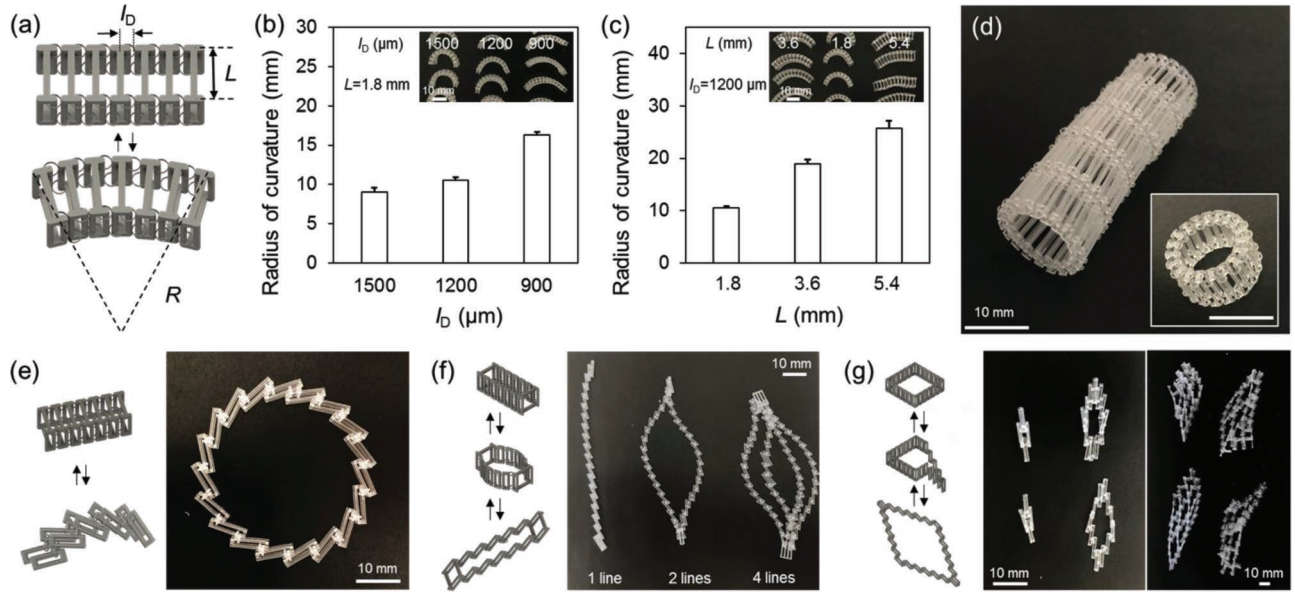

Figure 2. Assembly of NTTr units to fibers in a parallel configuration. a) Schematic images of two fibers in the bending motion. Radii of curvature for bent fibers with different geometries, b) l_D and c) L. The insets show microscopic images of bent fibers. Partially open loop hooks enable the fixation of stent-like tubular structures d) after the bending process, or e) after elongation and inclination. (f) NTTr units in a joined end configuration of two serial configurations form nets and meshes. g) NTTr units assembled in a rectangular configuration. The devices form a caged structure being stretched from a folded state to a rhomboidal shape.

fibers were connected together at each end, they transformed from an initially folded rectangular circuit to a rhomboidal shape circuit. By increasing the number of units in the single fibers, the area of the resulting rhomboidal structures increases (Figure 2g). Increasing the connecting points between the single fibers leads to finer meshes and higher mechanical stability of the resulting nets. Such structures might be applicable for medical mesh substrates or electrodes that can be wrapped around tissue. Catheter-inducible and transformable meshes are of great interest for heart-net electrodes to treat distention myocardiopathy, surgical meshes for hernia repair, neurosurgery tools to treat cerebral aneurysm, or inferior vena cava filters.

For such medical applications, the NTTr units should be processable with various types of materials at high scalability. All structures discussed so far were printed with a custom PEGDA-ITX-resin, which reaches high resolution in conventional 3D printing applications.[22] To show that other resins with different properties are applicable to our approach, the same NTTr design was printed with medically certified transparent printing materials: rigid medicalprint clear (MPC) and flexible luxaprint flex-resin (LFR). A comparison of the force applied for a continuous elongation and unfolding of the NTTr devices for structures printed from PEGDA-ITX, MPC, and LFR is shown in **Figure 3**a. Initially, all of the printed NTTr structures were smoothly transformed by the elongation. After being fully elongated, PEGDA-ITX- and MPC-printed structures failed due to breakage of the attachment loops. In contrast, the maximum elongation at break of LFR-printed structures was 21 ± 1%. Since LFR is a mixture of urethane acrylate oligomers, the attachment loops were able to bend, which resulted in an better force distribution and thus a higher elongation and force compliance (Figure S3, Supporting Information). It is expected that NTTr fibers made from more advanced photo-curable silicones and hydrogels will endow an even higher flexibility and porosity. This will facilitate the design of closely packed structures that can be introduced with narrow catheters and potentially be used for controlled drug release. Furthermore, the use of biodegradable resins will allow the fabrication of non-permanent implants.

To add functionality to the NTTr structures, we modified their surface with conducting materials. After sputtering the printed structures with gold (≈105 nm) the NTTr fibers became electrically conductive. The resistances between two edges of single $H = 2$ mm and double $H = 6$ mm fibers were measured to estimate the conductivity during shape transformation from the original state to shifted and inclined states (Figure 3b). Over the course of 9 cycles, we observed an increase of the resistance in the range of 4 orders of magnitude upon sliding and stretching the structure with 60% deformation and elongation. When fully bent, the resistance decreased back in the range of its initial value. We attribute the difference in resistance between the shifted and inclined state to a change in contact at the loop attachments and the rods. Potentially, the resin could be supported with conductive materials such as carbon or metal nanoparticles to improve the mechanical and electrical stability during the deformation.[23] Besides, the single units may be manufactured with embedded ferromagnetic particles or metal-sputtered polymers, which enables remotely transforming the shape by applying a magnetic field.[24]

We investigated the scaling of the process to smaller structures using PEGDA-ITX whose achievable resolution is higher than the other two resins. As shown in Figure 2d,e, two strands each containing 19 NTTr units in series with $L = 1.8$ mm and $I_D = 1200$ μm formed stent structures with radii of curvature (R) of ≈6 and 12 mm, depending on the applied shape

© 2021 The Authors. Advanced Materials Technologies published by Wiley-VCH GmbH

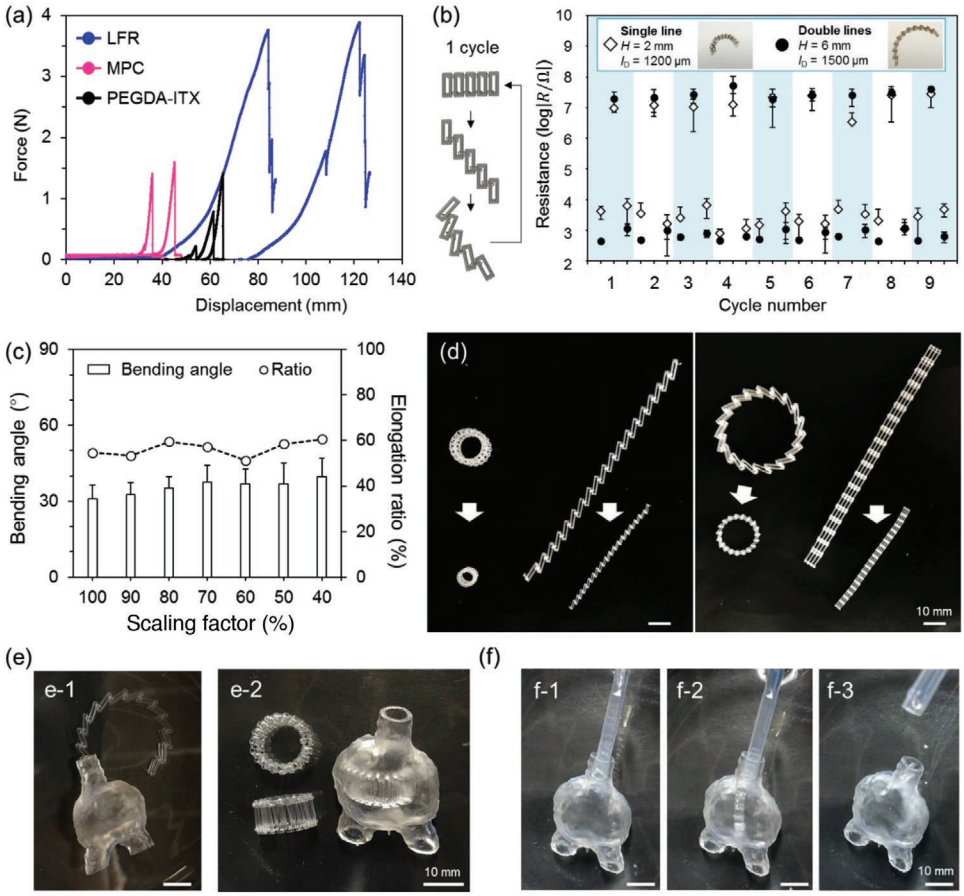

Figure 3. a) Tensile test of three types of materials: PEGDA-ITX (black), medicalprint clear (MPC; magenta), and luxaprint flex (LFR; blue). b) Conductivity of Au-sputtered NTTr fibers during three different deformation states. c) Inclination angles and elongation ratios of miniaturized 3D printed NTTr units. d) Bright field images of miniaturized tubular assembly. The fibers were arranged in d-1) two and d-2) four rows. Bent and connected shapes to form stent structures. e,f) Time-lapsed images of a vessel mock-up with manually inserted NTTr stent fibers e-1,e-2) with larger designs and f-1–f-3) fluidically inserted smaller designs.

transformation. Using the same DLP-based 3D-printer with 30 µm × 30 µm square pixel exposure grids, we printed the geometric structure in different sizes down to a minimum of 40% of its original value in 1D. Keeping the aspect ratio by applying a uniform scaling factor, this amounts to a final volume reduction of 93.6% (6.4% of the original volume). The inclination angles between two paired units and their elongation ratio remained approximately constant, regardless of the feature size (Figure 3c and Figure S4, Supporting Information). Since the achievable miniaturization is mainly dependent upon the resolution of the 3D printer and the polymerization and absorption efficiency of the resin, higher resolution printers such as 2 photon-microscopy lithography could further reduce the NTTr structures to the micron scale or below.[25]

The smallest tubular stents (6.4% in volume) were assembled while maintaining the same aspect ratio. We used a bending motion as well as inclination motion to generate differently sized stent structures, with small and large diameters, respectively (Figure 3d). With printed polyurethane vessel mock-ups, we demonstrated that the NTTr structures can be inserted in a vessel and transformed to a stent structure. Large structures (100% in volume) were arranged in two rows and directly inserted through a 5 mm vessel in the shifted state. Once inside, they were folded to form a stent-like structure at the bifurcation point (Figure 3e). After the structures were connected, they smoothly fit to the inner surface of the branched vessels with 78.5 mm in circumference. Furthermore, we demonstrated insertion of small fibers (6.4% in volume) that were arranged in four rows through a tube (Figure 3f). Once the elongated structure was sucked into the catheter-like tubes (inner-diameter of 4 mm), it could be introduced to the target vessel by flow injection. After full entry, the expanded fibers were manually inclined in order to reconstruct cylindrical stents and complete the deployment, while maintaining their elongated state.

Depending on the diameters of the target tissues, delivery catheter passages, or blood vessels, stents can be readily generated in a rapid prototyping approach. The final size of the stent is tunable with the assembly process, design parameters of single NTTr units, and the number of units or fibers. The NTTr devices form a tubular stent-like structure with partially open, reversible, and detachable coupler hooks. This makes it easy to dynamically switch between closely packed and expanded states and facilitates the retrieval of the stents after treatment.

© 2021 The Authors. Advanced Materials Technologies published by Wiley-VCH GmbH

3. Conclusion

In conclusion, we demonstrated the capability of 3D-printable and highly deformable NTTr structures and optimized them for potential application as implantable stents and meshes. The structure composed of two central rods and two attachment rings allowed a transformation from 1D fibers to 2D meshes or 3D tubular shapes. The 3D-printing technology allows the fabrication of interconnected assembled structures in a batch manner, at dimensions where manual assembly is impracticable. The deformation is mainly dependent on the geometry and position of attachments, which can be customized for a specific application. Both scalability and applicability to different materials broaden the potential for utilization. We envision that the 3D-printable NTTr devices provide the possibility for flexible design of medical implants such as stents and mesh supports.

Supporting Information

Supporting Information is available from the Wiley Online Library or from the author.

Acknowledgements

T.F.T. and L.H. contributed equally to this work. The authors would like to acknowledge Dr. Hitonobu Tomoike and Dr. Joe Alexander at NTT Research Incorporated for their helpful discussion. The authors also thank Mr. Tim Scherzer and Prof. Dr. Petra Mela at Technische Universität München for their assistance with tensile testing, and Dr. Hiroshi Nakashima and Mrs. Naoko Maekawa at NTT Basic Research Laboratories for the preparation of Nanjing Tamasudare tools.

Open access funding enabled and organized by Projekt DEAL.

Conflict of Interest

The authors declare no conflict of interest.

Data Availability Statement

Research data are not shared.

Keywords

3D printing, implants, shape transformation, stents

Received: February 27, 2021
Revised: April 23, 2021
Published online:

[1] D. H. Kim, J. Viventi, J. J. Amsden, J. Xiao, L. Vigeland, Y. S. Kim, J. A. Blanco, B. Panilaitis, E. S. Frechette, D. Contreras, D. L. Kaplan, F. G. Omenetto, Y. Huang, K. C. Hwang, M. R. Zakin, B. Litt, J. A. Rogers, *Nat. Mater.* **2010**, *9*, 511.

[2] a) J. P. Montgomery, J. A. Kaufman, *Semin. Interventional Radiol.* **2016**, *33*, 79; b) E. Folch, C. Keyes, *Ann. Cardiothorac. Surg.* **2018**, *7*, 273.

[3] A. Ghosh, L. Li, L. Xu, R. P. Dash, N. Gupta, J. Lam, Q. Jin, V. Akshintala, G. Pahapale, W. Liu, A. Sarkar, R. Rais, D. H. Gracias, F. M. Selaru, *Sci. Adv.* **2020**, *6*, eabb4133.

[4] C. Li, C. Guo, V. Fitzpatrick, A. Ibrahim, M. J. Zwierstra, P. Hanna, A. Lechtig, A. Nazarian, S. J. Lin, D. L. Kaplan, *Nat. Rev. Mater.* **2020**, *5*, 61.

[5] a) T. J. Oxley, N. L. Opie, S. E. John, G. S. Rind, S. M. Ronayne, T. L. Wheeler, J. W. Judy, A. J. McDonald, A. Dornom, T. J. Lovell, C. Steward, D. J. Garrett, B. A. Moffat, E. H. Lui, N. Yassi, B. C. Campbell, Y. T. Wong, K. E. Fox, E. S. Nurse, I. E. Bennett, S. H. Bauquier, K. A. Liyanage, N. R. van der Nagel, P. Perucca, A. Ahnood, K. P. Gill, B. Yan, L. Churilov, C. R. French, P. M. Desmond, M. K. Horne, L. Kiers, S. Prawer, S. M. Davis, A. N. Burkitt, P. J. Mitchell, D. B. Grayden, C. N. May, T. J. O'Brien, *Nat. Biotechnol.* **2016**, *34*, 320; b) N. L. Opie, S. E. John, G. S. Rind, S. M. Ronayne, Y. T. Wong, G. Gerboni, P. E. Yoo, T. J. H. Lovell, T. C. M. Scordas, S. L. Wilson, A. Dornom, T. Vale, T. J. O'Brien, D. B. Grayden, C. N. May, T. J. Oxley, *Nat. Biomed. Eng.* **2018**, *2*, 907.

[6] K. Kuribayashi, K. Tsuchiya, Z. You, D. Tomus, M. Umemoto, T. Ito, M. Sasaki, *Mater. Sci. Eng., A* **2006**, *419*, 131.

[7] X. Chen, B. Assadsangabi, Y. Hsiang, K. Takahata, *Adv. Sci.* **2018**, *5*, 1700560.

[8] a) Y. J. Hong, H. Jeong, K. W. Cho, N. Lu, D.-H. Kim, *Adv. Funct. Mater.* **2019**, *29*, 1808247; b) D. Son, J. Lee, D. J. Lee, R. Ghaffari, S. Yun, S. J. Kim, J. E. Lee, H. R. Cho, S. Yoon, S. Yang, S. Lee, S. Qiao, D. Ling, S. Shin, J. K. Song, J. Kim, T. Kim, H. Lee, J. Kim, M. Soh, N. Lee, C. S. Hwang, S. Nam, N. Lu, T. Hyeon, S. H. Choi, D. H. Kim, *ACS Nano* **2015**, *9*, 5937; c) D. H. Keum, J. H. Mun, B. W. Hwang, J. Kim, H. Kim, W. Jo, D. H. Ha, D. W. Cho, C. Kim, S. K. Hahn, *Small* **2017**, *13*, 1602925.

[9] G. I. Peterson, A. V. Dobrynin, M. L. Becker, *Adv. Healthcare Mater.* **2017**, *6*, 1700694.

[10] a) J. Liu, T. M. Fu, Z. Cheng, G. Hong, T. Zhou, L. Jin, M. Duvvuri, Z. Jiang, P. Kruskal, C. Xie, Z. Suo, Y. Fang, C. M. Lieber, *Nat. Nanotechnol.* **2015**, *10*, 629; b) T. Zhou, G. Hong, T. M. Fu, X. Yang, T. G. Schuhmann, R. D. Viveros, C. M. Lieber, *Proc. Natl. Acad. Sci. U. S. A.* **2017**, *114*, 5894.

[11] a) Q. Ge, C. K. Dunn, H. J. Qi, M. L. Dunn, *Smart Mater. Struct.* **2014**, *23*, 094007; b) G. Liu, Y. Zhao, G. Wu, J. Lu, *Sci. Adv.* **2018**, *4*, eaat0641.

[12] T. Kim, Y. G. Lee, *Sci. Rep.* **2018**, *8*, 13911.

[13] a) M. Zarek, N. Mansour, S. Shapira, D. Cohn, *Macromol. Rapid Commun.* **2017**, *38*, 1600628; b) M. S. Cabrera, B. Sanders, O. Goor, A. Driessen-Mol, C. W. J. Oomens, F. P. T. Baaijens, *3D Print. Addit. Manuf.* **2017**, *4*, 19; c) H. Jia, S.-Y. Gu, K. Chang, *Adv. Polym. Technol.* **2018**, *37*, 3222.

[14] L. Y. Zhou, J. Fu, Y. He, *Adv. Funct. Mater.* **2020**, *30*, 2000187.

[15] a) Q. Zhou, T. Petit, H. Choi, B. J. Nelson, L. Zhang, *Adv. Funct. Mater.* **2017**, *27*, 1604571; b) S. Kim, F. Qiu, S. Kim, A. Ghanbari, C. Moon, L. Zhang, B. J. Nelson, H. Choi, *Adv. Mater.* **2013**, *25*, 5863; c) M. R. Gullo, S. Takeuchi, O. Paul, *Adv. Healthcare Mater.* **2017**, *6*, 1601053.

[16] A. P. Kuo, N. Bhattacharjee, Y. Lee, K. Castro, Y. T. Kim, A. Folch, *Adv. Mater. Technol.* **2019**, *4*, 1800395.

[17] B. S. Jang, J. E. Jeong, S. Ji, D. Im, M. K. Lee, S. A. Park, W. H. Park, *Mater. Des.* **2020**, *195*, 109005.

[18] J. Xu, H. X. Ong, D. Traini, M. Byrom, J. Williamson, P. M. Young, *Drug Dev. Ind. Pharm.* **2019**, *45*, 1.

[19] P. Fouladian, J. Kohlhagen, M. Arafat, F. Afinjuomo, N. Workman, A. Y. Abuhelwa, Y. Song, S. Garg, A. Blencowe, *Biomater. Sci.* **2020**, *8*, 6625.

[20] P. Fathi, G. Capron, I. Tripathi, S. Misra, F. Ostadhossein, L. Selmic, B. Rowitz, D. Pan, *Biomaterials* **2020**, *228*, 119542.

© 2021 The Authors. Advanced Materials Technologies published by Wiley-VCH GmbH

[21] M. Kaya, A. Gacar, B. Demirci, S. M. Soylu, M. Y. Gulbahar, *J. Avian Med. Surg.* **2015**, *29*, 136.
[22] S. Zips, L. Hiendlmeier, L. J. K. Weiß, H. Url, T. F. Teshima, R. Schmid, M. Eblenkamp, P. Mela, B. Wolfrum, *ACS Appl. Polym. Mater.* **2021**, *3*, 243.
[23] a) K. Terkan, F. Zurita, T. J. Khalaf, P. Rinklin, T. F. Teshima, T. Kohl, B. Wolfrum, *APL Mater.* **2020**, *8*, 101111; b) J. T. Muth, D. M. Vogt, R. L. Truby, Y. Mengüç, D. B. Kolesky, R. J. Wood, J. A. Lewis, *Adv. Mater.* **2014**, *26*, 6307; c) H. W. Tan, J. An, C. K. Chua, T. Tran, *Adv. Electron. Mater.* **2019**, *5*, 1800831.
[24] a) S. Lantean, G. Barrera, C. F. Pirri, P. Tiberto, M. Sangermano, I. Roppolo, G. Rizza, *Adv. Mater. Technol.* **2019**, *4*, 1900505; b) T. Teshima, H. Onoe, H. Aonuma, K. Kuribayashi-Shigetomi, K. Kamiya, T. Tonooka, H. Kanuka, S. Takeuchi, *Adv. Mater.* **2014**, *26*, 2850.
[25] E. Kim, S. Jeon, H. K. An, M. Kianpour, S. W. Yu, J. Y. Kim, J. C. Rah, H. Choi, *Sci. Adv.* **2020**, *6*, eabb5696.

© 2021 The Authors. Advanced Materials Technologies published by Wiley-VCH GmbH